RM L57D24b

NACA

RESEARCH MEMORANDUM

STEADY LOADS DUE TO JET INTERFERENCE ON WINGS, TAILS, AND FUSELAGES AT TRANSONIC SPEEDS

By John M. Swihart and Norman L. Crabill

Langley Aeronautical Laboratory
Langley Field, Va.

NATIONAL ADVISORY COMMITTEE
FOR AERONAUTICS

WASHINGTON

May 22, 1957
Declassified October 28, 1960

NATIONAL ADVISORY COMMITTEE FOR AERONAUTICS

RESEARCH MEMORANDUM

STEADY LOADS DUE TO JET INTERFERENCE ON WINGS, TAILS, AND FUSELAGES AT TRANSONIC SPEEDS

By John M. Swihart and Norman L. Crabill

SUMMARY

This paper gives the results of some recent investigations of jet-interference effects on actual airplane configurations at transonic speeds. Data presented herein were obtained with hot jets on both wind-tunnel and flight models. Results indicate that jet-induced effects are small at subsonic speeds; however, at low supersonic Mach numbers, these effects are comparable to those obtained at substantially higher Mach numbers.

INTRODUCTION

In recent years there have been several investigations of turbojet-exhaust interference effects at supersonic speeds (refs. 1 and 2); however, only a limited amount of data has been obtained at transonic speeds. It is the purpose of this paper to show the results of some recent investigations of the jet interference on actual airplane configurations at transonic speeds. This discussion will be limited to steady loads induced by simulated jets on nearby wings, tails, and overhanging fuselages. Data presented in this paper cover the Mach number range of 0.85 to 1.20 and were obtained with hot jets at total pressure ratios corresponding to current turbojet-engine pressure ratios.

SYMBOLS

b	span
c	local chord
$\bar{c}$	mean aerodynamic chord
c_n	section normal-force coefficient
C_N	normal-force coefficient

ΔC_N incremental normal-force coefficient, $C_{N,\text{jet on}} - C_{N,\text{jet off}}$

C_p pressure coefficient, $\frac{p_{local} - p_\infty}{q}$

ΔC_p incremental pressure coefficient, $C_{p,\text{jet on}} - C_{p,\text{jet off}}$

d_j primary jet diameter

p pressure

q dynamic pressure

y spanwise distance

z distance below wing chord plane

Subscripts:

AV average

j jet

R resultant, Lower surface - Upper surface

t total

T tail

∞ free stream

APPARATUS

The models used in these investigations are shown in figure 1. The sting-mounted 60° delta-wing model was tested in the Langley 16-foot transonic tunnel with one jet nacelle located at 41 and 69 percent of the semispan on one wing panel only. At the inboard station, the jet exit was located at 38 and 69 percent of the local chord and at 1, 2, and 4 jet diameters below the wing. At the outboard location, the nacelle was tested only at 4 jet diameters below the wing, and the exit was at 63 percent of the local chord. Simulation of the exhaust of a non-afterburning turbojet engine was achieved through the use of a hydrogen peroxide gas generator exhausting through a sonic exit. The jet total pressure ratio was 1 (power off) and 5 with a jet stagnation temperature of about 1,400° F at each test Mach number. Pressures were measured by static orifices located at about every 5 percent of the chord on the upper and lower surfaces at six spanwise stations.

The twin-engine model with part of the fuselage overhanging the jet exhaust was also a 16-foot-transonic-tunnel model and was supported at the wing tips by a bifurcate sting-support system. Two hydrogen peroxide turbojet simulators were mounted in arm-pit nacelles; their exhausts were partially separated by a short keel. Static pressures were measured along this keel and the shoulder of the overhanging fuselage. The horizontal tail was mounted in both a high position (on the vertical tail) and a relatively low position (on the boom). Pressure distributions were obtained on both tails directly above the jet center line extended.

The single-engine model with the fuselage overhang was flight tested with the horizontal tail located ahead of the jet exit and at two positions downstream of the jet exit. An afterburning turbojet engine was simulated by using a solid-propellant rocket motor exhausting through a sonic exit at a total pressure ratio of 6.0 and a stagnation temperature of 3,200° F. Pressures were measured on the top and bottom of the fuselage overhang and at two spanwise stations on the tails at a Mach number of 1.2.

An investigation was conducted in the Langley 16-foot transonic tunnel of a target-type thrust reverser mounted on a single-engine fighter model to evaluate the thrust reverser as a speed brake. The design of the reverser was taken from reference 3, and the jet exhaust was simulated by a hydrogen peroxide simulator operating at a jet total pressure ratio of 5. During the course of this investigation, static pressures were measured around half of the fuselage at 6 meridians and for about 3 jet diameters ahead of the base. Flow visualization was achieved by tufts on the other half of the fuselage.

Data are presented for the wind-tunnel models from $M = 0.85$ to 1.05; data are presented for the flight model at $M = 1.20$.

RESULTS AND DISCUSSION

Effects of Isolated Jets

Before discussing the results of these tests, a review will be given of the phenomena pertinent to the exhaust of an isolated overpressure sonic jet into subsonic and supersonic external streams. At current jet total pressure ratios, the jet bulges outward immediately downstream of the jet exit at both Mach numbers (fig. 2). At subsonic speeds, since the internal structure of shocks and expansions cannot penetrate the subsonic mixing boundary (see ref. 4), the only significant effects in the external flow are some compression due to the bulge near the exit and a subsequent expansion downstream due to entrainment of the external stream by the jet (fig. 2). Contrariwise, for supersonic speeds, Leiss

and Bressette (ref. 1), Love and Grigsby (ref. 4), and others have shown that the external flow is marked by a shock at the initial bulge (exit shock), an expansion over the curved jet boundary, and a shock (jet shock) which occurs where the shock internal to the jet penetrates the supersonic mixing boundary (fig. 2). Even though the initial deflection angle of the bulge is only about half that for subsonic speeds (ref. 4), the presence of shocks in the external flow indicates that the effects on the external stream may be considerably larger than in subsonic flow and probably extend to greater distances from the jet boundary.

Jet Effects on Wings

Figure 3 shows the jet-induced resultant pressures on the 60° delta-wing model at $M = 0.90$ and 1.05 for $\alpha = 5^\circ$ for one nacelle located 1 jet diameter below the right wing and with the jet exit at 69 percent of the local chord. Qualitatively, the results are about what might be expected from the discussion given for isolated jets (fig. 2). At $M = 0.90$, the effects of flow inclination near the jet exit and the subsequent expansion due to entrainment produce $\Delta C_{p,R}$ peaks of no more than 0.09 and -0.05, respectively. At $M = 1.05$, the effect of the exit shock is to give a positive peak of $\Delta C_{p,R} = 0.27$; the negative peak is slightly less than 0.10. The effects diminish rapidly with increasing spanwise distance from the jet at $M = 0.90$ and only moderately at $M = 1.05$.

Figure 4 presents jet-induced resultant pressures for the same test conditions as those for figure 3 except the whole nacelle has been moved down to $\frac{z}{d_j} = 4$ and forward so that the exit is now at 38 percent of the local chord. In general, the jet effects are shifted correspondingly forward and, at $M = 0.90$, the effects are somewhat diminished. At $M = 1.05$, however, the maximums and minimums are comparable with those obtained when the nacelle was located only 1 jet diameter below the wing (fig. 3) as far as the exit shock intersects the wing. The data indicate that the exit shock has passed off the leading edge of the wing slightly outboard of $\frac{y}{b/2} = 65$ percent and that the jet effect shown for $\frac{y}{b/2} = 74$ percent comes entirely from the influence of the jet on the wing upper-surface pressures. Evidently, this effect results from some interaction of the jet-exit shock and the wing leading edge.

The chordwise pressure distributions obtained at $\alpha = 5^\circ$ and $M = 0.90$ and 1.05 for the two nacelle positions shown in figures 3 and 4 have been integrated to obtain the spanwise loading curves shown in figure 5. Additional data obtained for the nacelle located at 69 percent of the wing semispan with the jet exit at 63 percent of the local chord and 4 jet diameters below the wing are given in figure 6. Spanwise loadings for the basic wing (no nacelle or pylon) are also given in

figures 5 and 6 for comparison. It is seen that the largest effects occur at $M = 1.05$ in all three cases, and that, at this Mach number, the effect is smallest for the case where the exit-shock intercept passes off the wing before reaching the tip. Although the $\Delta C_N = 0.010$ measured for the nacelle positioned at the inboard location and 1 jet diameter below the wing is only about 5 percent of the wing normal force, it is actually about 1.5 times the thrust of the jet causing this effect. This is comparable in magnitude to the effects shown in reference 1 at a Mach number of 1.8.

The wing chordwise and spanwise center-of-pressure locations for the nacelle located at the inboard position and for $z/d_j = 1$ and 4 are shown in figure 7. Jet operation has a very small effect on the chordwise center of pressure and practically no effect on the spanwise center of pressure at subsonic speeds. In general, the data indicate that the slight forward and inboard movement of the center of pressure is more pronounced for $z/d_j = 1$.

Jet Effects on Fuselage Overhangs and Horizontal-Tail Surfaces

The data shown in figure 8 give the effect of Mach number on jet-induced pressures measured along the overhanging portions of two different exit configurations. Although these data were obtained on two different configurations at different jet total pressure ratios, these differences are unimportant in showing the effects that are discussed here. For the data at $M = 0.85$ (the twin-engine fighter), the increment of $\Delta C_p = 0.25$ at the center line indicates that the jet is probably in contact with the center-line row of orifices over the entire length of the short keel; however, very little jet effects were measured at the orifice row around the shoulder. Extensive pressure surveys of this kind have been shown in reference 5.

At $M = 1.20$, the data (the single-engine type) indicate that the orifices on the bottom of the boom were probably in contact with the jet at least near the exit. The pressure measurements made along the top of the boom when the horizontal tail was located ahead of the exit indicate that moderate positive pressure increments are experienced even though this position is "blanketed" by the boom. Additional data, not shown here, indicate that the leading edge of this upper-surface jet-effect zone moves aft with increasing Mach number.

Thus, at subsonic speeds, the region of fuselage overhangs subject to significant jet effects is nearly confined to that in contact with the jet. At supersonic speeds, the region of significant jet effects extends much further away from the jet boundary and can even affect blanketed areas.

The effect of tail position on the jet-induced tail chordwise pressure distributions measured at $M = 1.20$ on the single-engine model is shown in figure 9. The data indicate that the loading over the forward third of the tail is greatest for the forward tail position and that the loading is greater outboard. The lower loading at the inboard location may be due to the effects of a subsonic jet mixing boundary in the region immediately under the boom and this subsonic mixing boundary may give way to a supersonic mixing boundary outboard, with consequent increase in jet effects.

Figure 10 shows the effect of tail position and free-stream Mach number on jet-induced tail and tail-plus-afterbody normal-force coefficients. Pressure distributions obtained for the high and low horizontal tails at $M = 0.85$ on the twin-engine model were integrated to obtain the jet-induced effect on section normal-force coefficient as a function of angle of attack. The data indicate that for the high tail there is no jet effect on c_n at any angle of attack, whereas, in the low tail position, a constant reduction of 0.07 in c_n was obtained at all angles of attack. This result indicates that the flow entrainment effect of a jet in subsonic flow diminishes rapidly with distance from the jet boundary.

Accelerometer data taken at $M = 1.20$ for the three longitudinal positions of the horizontal tail on the single-engine models were reduced to show ΔC_N induced by the jet on the afterbody and afterbody plus tail. The data, based on the plan-form area downstream of the jet, indicate that ΔC_N probably goes through a maximum as the position of the exposed tail centroid is varied between 0 and 2.3 jet diameters downstream of the jet exit. If the reduction in tail-section normal-force coefficient obtained at $M = 0.85$ be taken as representative of the effect over the entire tail, then the total jet-induced tail loads are seen to change sign as the free-stream Mach number is increased from $M = 0.85$ to 1.20.

Jet Effects Due to Thrust Reverser

The effect of thrust-reverser operation on afterbody pressures on a single-engine blunt-based fighter-type configuration flying at $M = 1.05$ is given in figure 11. The curves shown represent averages of the six pressures measured around the periphery of the left side of the afterbody at each fuselage station. When no reverser is present, the pressures ahead of the base are negative and decrease to -0.27 at the base. When the target-type reverser was extended, the pressures were increased to positive values for about 3 jet diameters ahead of the base. The tuft studies indicated that separation occurred on the fuselage forward of 3 jet diameters and this separation was very unstable. The resulting large lateral oscillations of the model on the relatively rigid support system used in the wind-tunnel test indicate that the operation of this

device on an airplane in free flight might render the airplane unflyable. Although it is now known that this reverser is not a good design, it is believed that the magnitude of these local pressure changes is typical of what should be expected with most thrust reversers.

CONCLUSIONS

Examination of the data from recent investigations of jet-interference effects on actual airplane configurations at transonic speeds has led to the following tentative conclusions:

1. At subsonic speeds, jet-induced effects on wings, tails, and fuselages are small and decrease rapidly with distance from the jet boundary.

2. At low supersonic Mach numbers, jet-induced effects comparable to those obtained previously at substantially higher Mach numbers can be realized. Generally, these effects do not diminish as rapidly with distance from the jet boundary as those induced in subsonic flow.

Langley Aeronautical Laboratory,
National Advisory Committee for Aeronautics,
Langley Field, Va., March 5, 1957.

REFERENCES

1. Leiss, Abraham, and Bresette, Walter E.: Pressure Distribution Induced on a Flat Plate by a Supersonic and Sonic Jet Exhaust at a Free-Stream Mach Number of 1.80. NACA RM L56I06, 1957.

2. Rainey, Robert W.: The Effects Upon Body Drag of Jets Exhausting From Wing-Mounted Nacelles. NACA RM L56A09, 1956.

3. Povolny, John H., Steffen, Fred W., and McArdle, Jack G.: Summary of Scale-Model Thrust-Reverser Investigation. NACA TN 3664, 1956.

4. Love, Eugene S., and Grigsby, Carl E.: Some Studies of Axisymmetric Free Jets Exhausting From Sonic and Supersonic Nozzles Into Still Air and Into Supersonic Streams. NACA RM L54L31, 1955.

5. Cornette, Elden S., and Ward, Donald H.: Transonic Wind-Tunnel Investigation of the Effects of a Heated Propulsive Jet on the Pressure Distribution Along a Fuselage Overhang. NACA RM L56A27, 1956.

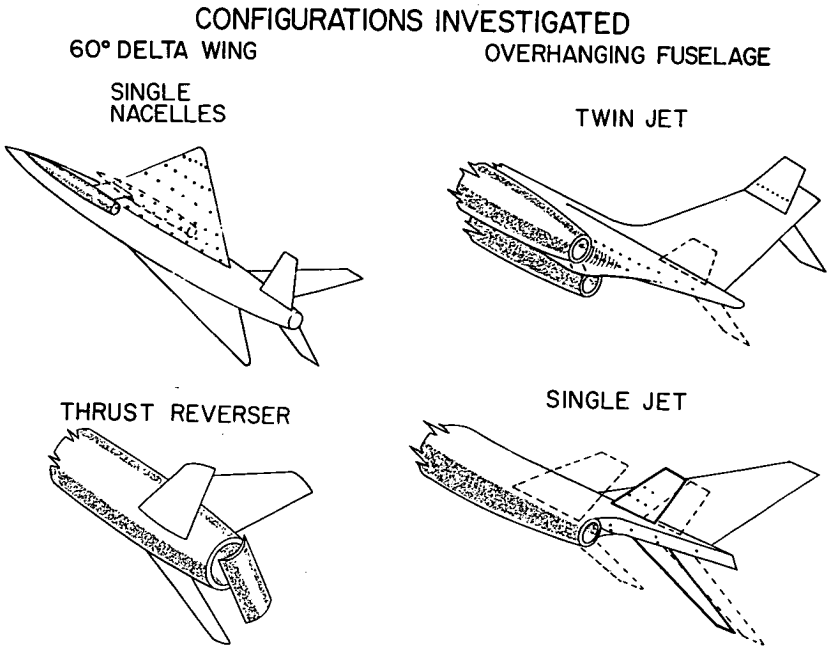

Figure 1

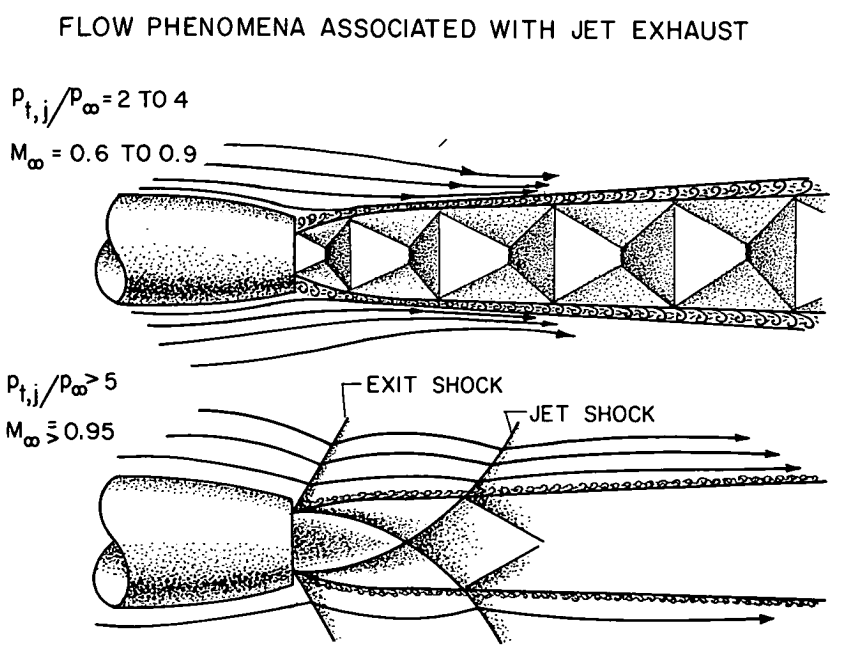

Figure 2

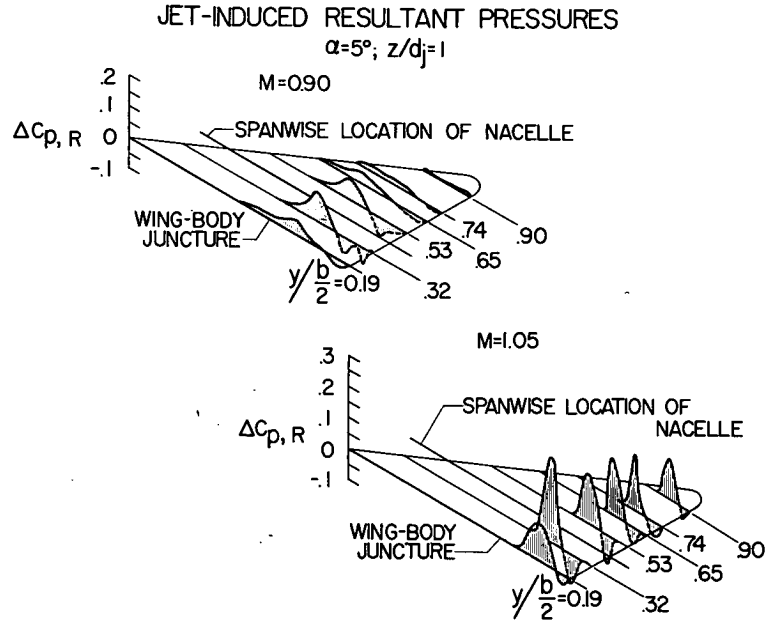

Figure 3

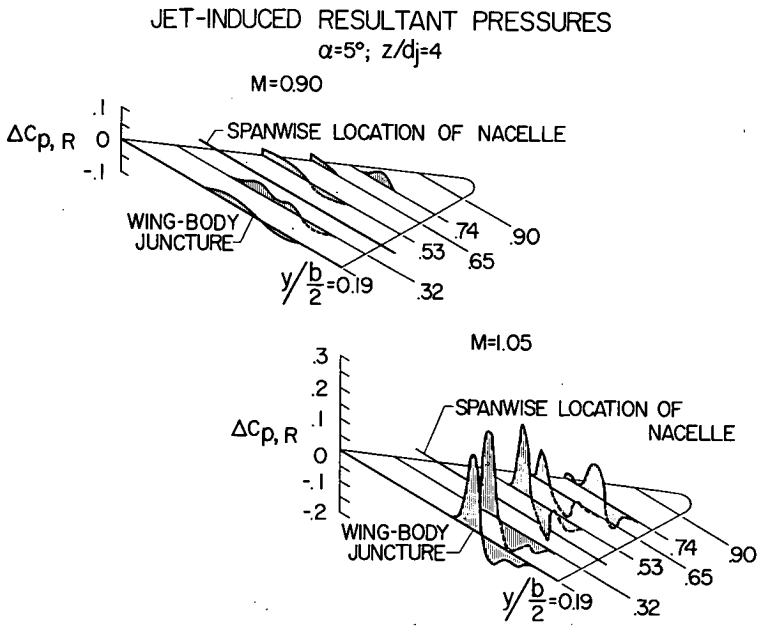

Figure 4

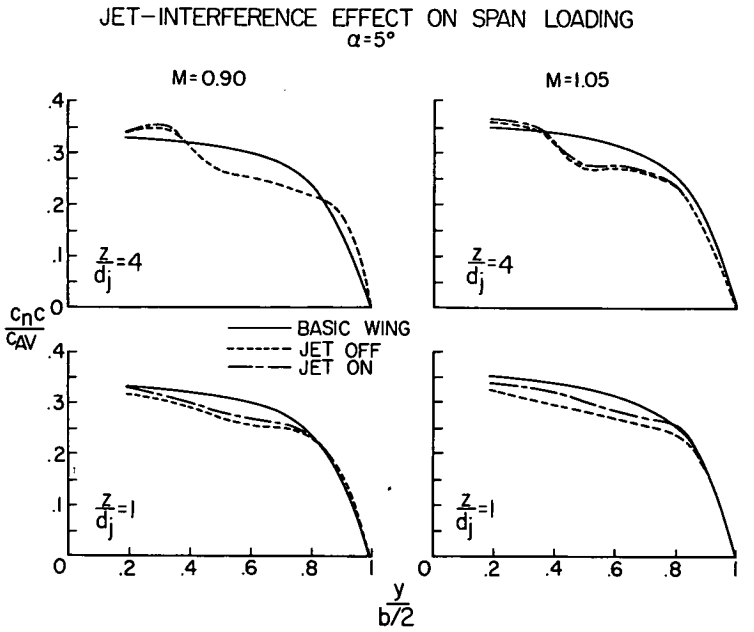

Figure 5

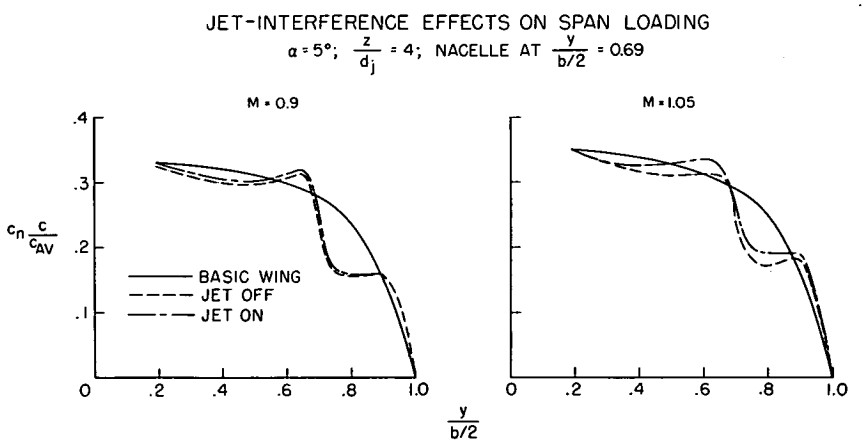

Figure 6

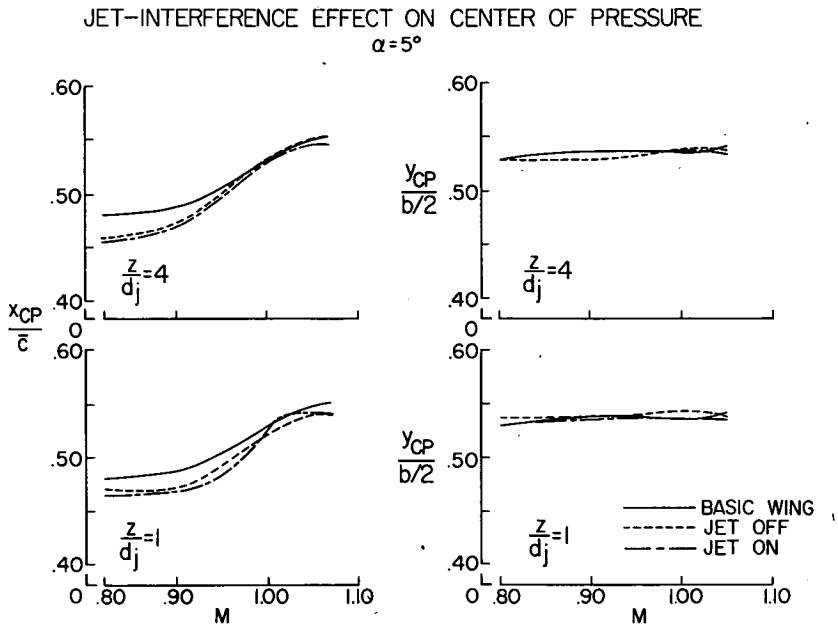

Figure 7

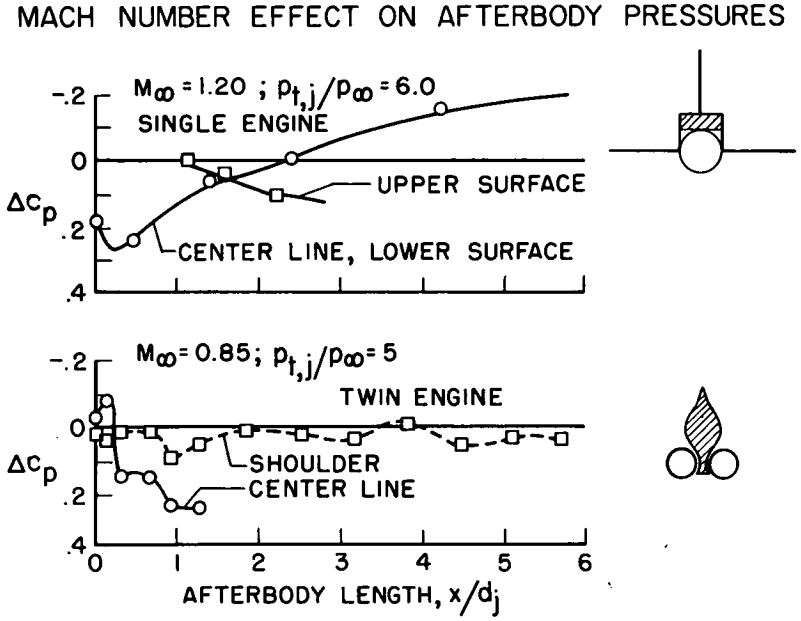

Figure 8

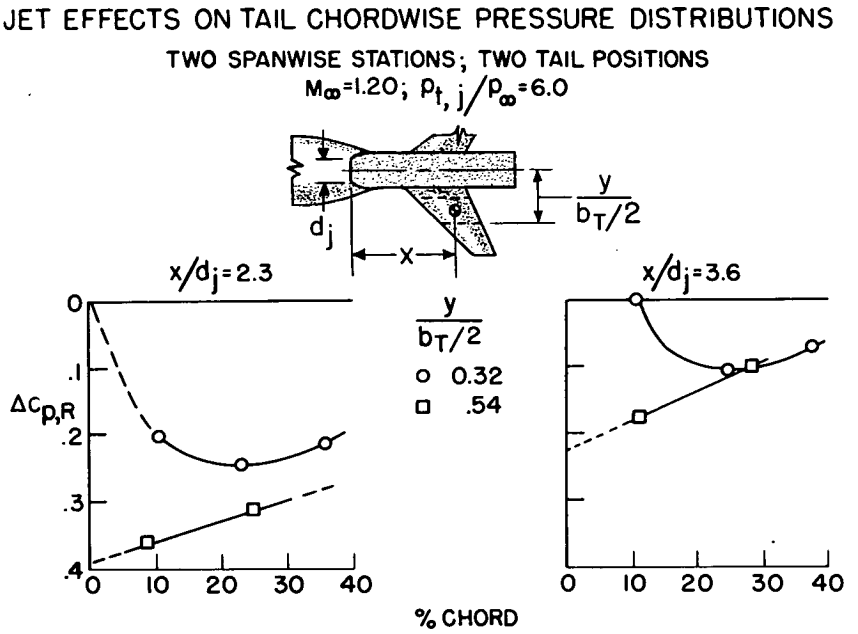

Figure 9

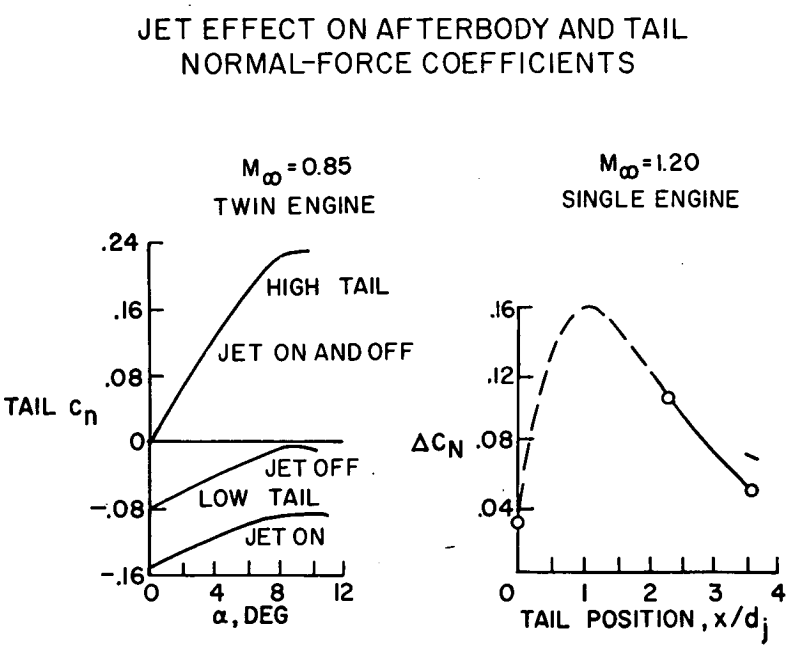

Figure 10

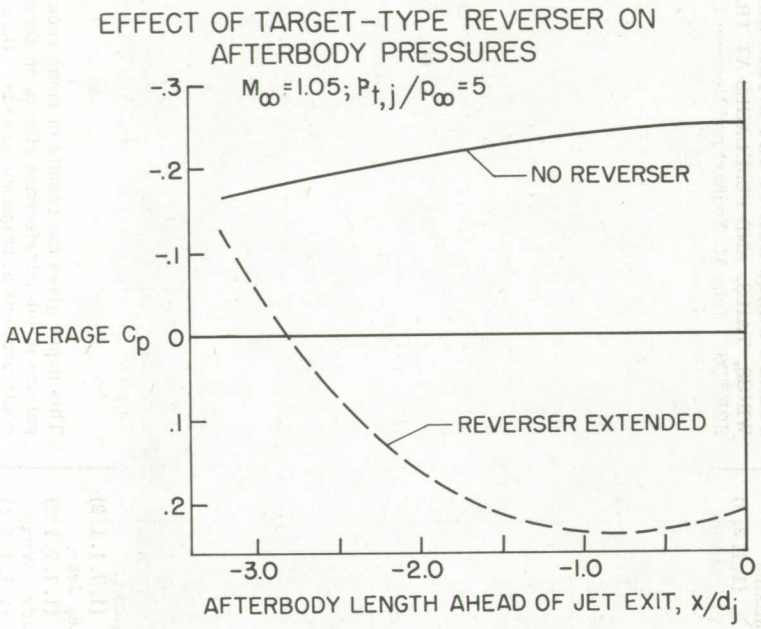
EFFECT OF TARGET-TYPE REVERSER ON AFTERBODY PRESSURES
$M_\infty = 1.05$; $P_{t,j}/p_\infty = 5$
NO REVERSER
REVERSER EXTENDED
AVERAGE C_p
-.3
-.2
-.1
0
.1
.2
-3.0
-2.0
-1.0
0
AFTERBODY LENGTH AHEAD OF JET EXIT, x/d_j

Figure 11